THE SPANWISE DISTRIBUTION OF LOSSES IN PRISMATIC TURBINE CASCADE WITH NON-UNIFORM INLET VELOCITY PROFILE

Jiří Fürst*, Martin Luxa**, David Šimurda**

The paper deals with the experimental and numerical research of flows through prismatic turbine cascade in transonic regimes. The primary goal is to evaluate the influence of the non-uniformity of the inlet velocity profile to the span-wise distribution of energy losses. The numerical simulation with inlet velocity profile corresponding to the parameters of the flow in high speed wind tunnel in Nový Knín is compared with the experimental data.

Keywords: *prismatic turbine cascade, losses, velocity profile*

1. Introduction

The flow through a turbine cascade is influenced by the interaction with end walls. The secondary flows comming from the development of the end-wall boundary layers cause additional losses which affects the overall performance of the turbine cascade. The problem of secondary flows is discussed in the literature, for a review see Lampart [7], Sieverding [12]. The complex flow structure of the secondary flows leads to non-trivial distribution of energy losses past the turbine blades. The pitch-averaged loss distribution possess usually local maxima at certain distance from the end-walls. Moreover, the non-uniformity of the flow field causes also the changes in the exit flow angle.

The effects of blade geometry and some flow parameters on the losses in subsonic axial turbines were investigated e.g. by Lampart [8]. In the case of flows with supersonic exit velocities one has to account for the additional 3D effects originating from the interaction of the shock waves with the non-uniform flow field in the vicinity of end-walls.

Present contribution is focused on the secondary flow structure and the distribution of energy losses and flow angles in the transonic turbine blade cascade SE1050. The previous study of Fürst, Luxa, and Šimurda [3] demonstrated that the span-wise distribution of losses strongly depends on the thickness of the boundary layer in the inlet channel. The present study shows that the effect of inlet boundary layer thickness is much more important than the choice of the turbulence model in this case.

2. Test Blade Cascade

The turbine cascade SE1050 is a freely available test case for transonic flows in turbomachinery, see Kozel and Příhoda [5], Šťastný and Šafařík [17]. The profile was designed

* doc. Ing. J. Fürst, PhD., Fac. of Mech. Eng., Czech Technical University in Prague, Karlovo nám. 13, 121 35 Prague, CZ

** Ing. M. Luxa, PhD., Ing. D. Šimurda, PhD., Institute of Thermomechanics AS CR, v.v.i., Dolejškova 1402/5, 182 00 Praha 8, CZ

for 1085 mm long rotor blade of the last turbine stage and it represents section located at the distance 320 mm from the root. Characteristic dimensions of the blade cascade model are apparent from Figure 1 and Table 1, respectively. Profile coordinates may be found in Kozel and Příhoda [5].

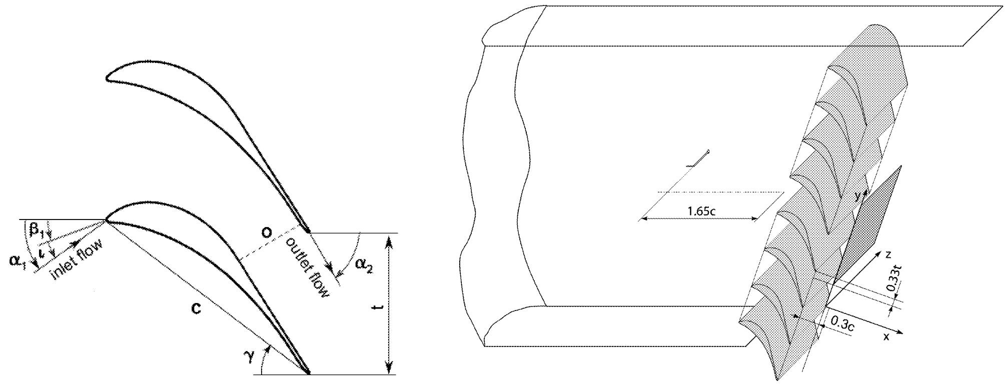

Fig.1: The scheme of the cascade (left) and the sketch of the test cascade (right)

Pitch	t	55.12 mm
Chord	c	100.0 mm
Throat	o	28.1 mm
Stagger Angle	γ	37.11°
Inlet Metal Angle	β_1	19.3°
Incidence	i	0.0°
Blade length	h	160.0 mm

Tab.1: Geometry of the cascade

All measurements were performed in the suction-type high-speed wind tunnel stationed in the Aerodynamic Laboratory of the Institute of Thermomechanics AS CR, v.v.i. in Nový Knín. During measurements, the tested blade cascade was fixed to sidewalls of a rotatable test section. Parameters of the inlet flow were measured by the Prandtl probe and three static pressure taps on the side-wall of the test section. Distributions of static pressure $p_2(z, y)$, total pressure $p_{t2}(z, y)$, pitch angle $\alpha_2(z, y)$ and yaw angle $\gamma_2(z, y)$ in the exit flow field were measured in the traversing plane located $0.3c$ behind the trailing edge plane. The traversed region covered two pitches and spanned over 140 mm of the 160 mm wide test section. For each of the two investigated regimes, measurements consisted of 17 pitchwise continuous traverses with 10 mm spanwise spacing in the center and 5 mm spacing at the edges of the traversing plane. Exit flow field distributions were measured using a traversing device with calibrated five-hole conical probe. The traversing device was equipped with PID controller, which utilizes pressure difference from the two vertically located pressure taps of the five-hole conical probe and sets the probe against the flow. The pitch angle was then measured by an angular transducer.

The accuracy of the measuring equipment enables us to measure the kinetic energy loss coefficient $\zeta = 1 - \lambda_2^2/\lambda_{2\mathrm{is}}^2$, where λ is the velocity magnitude related to the critical sound speed, with absolute uncertainty less than 0.4%, the pitch angle α_2 and the yaw angle

γ_2 with absolute uncertainty less than 1°. Periodicity of the exit flow field was assessed using so called 'Sliding data reduction method', see Matějka et al. [10] and the span-wise distribution of ζ was obtained using the data reduction method developed by Šafařík et al. [16]. Distribution of loss coefficient ζ in the midsection evaluated by this method ranged within band of width 0.005 and analogical distribution of exit flow angle ranged in band of width 7°. This aperiodicity in exit flow angle probably results from relatively low number of blades, see Luxa et al. [9].

The inlet velocity profile have been formed thanks to the relatively very long inlet channel placed upstream the cascade. The total pressure distribution across the channel $p_{1t} = f(z)$ was measured by a special shaped Pitot pressure probe, that is suitable also for measurement near the sidewall. The inlet velocity profile was then calculated using isentropic relations, see Fürst, Luxa, and Šimurda [3].

3. Numerical simulations

The flow through the turbine cascade was modelled using the system of time-averaged Navier-Stokes equations for compressible flows, see e.g. Ferziger and Peric [2]:

$$\frac{\partial \rho}{\partial t} + \frac{\partial (\rho\, u_j)}{\partial x_j} = 0\ , \tag{1}$$

$$\frac{\partial (\rho\, u_i)}{\partial t} + \frac{\partial (\rho\, u_i\, u_j)}{\partial x_j} + \frac{\partial p}{\partial x_i} = \frac{\partial (t_{ij} + \tau_{ij})}{\partial x_j}, \tag{2}$$

$$\frac{\partial (\rho\, E)}{\partial t} + \frac{\partial [(\rho\, E + p)\, u_j]}{\partial x_j} = \frac{\partial}{\partial x_j}\left[u_i\,(t_{ij} + \tau_{ij}) + \left(\frac{\mu}{Pr} + \rho\,\alpha_\theta\right)\frac{\partial h}{\partial x_j}\right]\ , \tag{3}$$

where ρ is the density, u_i are the components of the velocity vector, p is the static pressure, E is the specific total energy, $h = E + p - u_i\, u_i/2$ is the specific enthalpy, t_{ij} is the viscous stress tensor, $\tau_{ij} = -\overline{\rho\, u'_i\, u'_j}$ is the Reynolds stress tensor, μ is the viscosity, Pr is the Prandtl number, and α_θ is the turbulent thermal diffusivity. The perfect gas (the air) with $p = (\kappa - 1)(\rho\, E - \rho\, u_i\, u_i/2)$ where $\kappa = 1.4$ is the constant specific heat ratio is assumed. The flow is Newtonian with constant viscosity μ, hence $t_{ij} = 2\,\mu\,(S_{ij} - S_{ll}\,\delta_{ij}/3)$ where $S_{ij} = (\partial u_i/\partial x_j + \partial u_j/\partial x_i)/2$. The Reynolds stress tensor is approximated using several turbulence models:

- the SST turbulence model by Menter [11],
- the updated $k - \omega$ model by Wilcox [15],
- the TNT (i.e. *turbulent/non-turbulent*) $k-\omega$ model developed by Kok [4] with vortex modification by Brandsma et al. [1], and
- the explicit algebraic Reynolds stress model (EARSM) by Wallin [14].

The numerical solution was obtained with the finite volume method, namely with in-house develped modification of `rhoSimpleFOAM` solver from freely available `OpenFOAM` package. The solver uses segregated approach (SIMPLE loop) and employs limited second-order interpolations.

The simulation was carried out assuming the periodicity in pitch-wise direction and symmetry in span-wise direction. The inlet plane was located $0.25\,c$ before the leading edge and the outlet plane was at axial distance $0.5\,c$ behind the trailing edge. The average static pressure corresponding to given regime with isentropic outlet Mach number $M_{2\mathrm{is}} = 1.198$ was prescribed at the outlet plane. The distribution of total pressure corresponding to experimental setup was prescribed at the inlet plane together with constant value of total temperature and flow direction. The total pressure profile was modelled as

$$p_{1t}(z) = p_{\mathrm{ref}} \left[\frac{1 + \dfrac{\kappa - 1}{2}\, M_1(z)^2}{1 + \dfrac{\kappa - 1}{2}\, M_{\mathrm{ref}}^2} \right]^{\frac{\kappa}{\kappa-1}} , \tag{4}$$

where $M_{\mathrm{ref}} = 0.35$, $M_1(z) = M_{\mathrm{ref}} \min(z/\delta, 1)^{1/7}$, $p_{\mathrm{ref}} = 1{\times}10^5\,\mathrm{Pa}$, and δ is the inlet boundary layer thickness. The Reynolds number was $Re_{2\mathrm{is}} = 1.5{\times}10^6$, the inlet turbulence intensity was $Tu = 2\,\%$ and the inlet specific dissipation rate was $\omega = 10\,400\,\mathrm{s}^{-1}$

The 3D calculation has been carried out using an unstructured mesh with $3.3{\times}10^6$ prismatic/hexahedral cells with mesh refinement in the vicinity of walls giving mesh with first cell bellow $y_1^+ < 1$. In order to check the mesh-independence of results the additional computations were carried out using coarser mesh (see Fürst, Luxa, and Šimurda [3]) and using locally refined mesh with refinement near the shock waves and in the regions with increased entropy.

3.1. Numerical results

The figure 2 shows the isolines of the Mach number in the symmetry plane ($z = 80\,\mathrm{mm}$) obtained with OpenFOAM using the unstructured mesh and the mesh with local refinement. Although the results obtained with refined mesh capture better the wake and shock wave, the structure of flow field is quite well resolved even using the original unstructured mesh.

The figure 3 shows the iso-lines of local kinetic energy loss coefficient ζ and the structure of secondary flows in the traversing plane past the cascade. One can see that the differences between all four turbulence models are very small in this case. This is in some sense in contradiction to results presented by Kozel, Louda, and Příhoda [6] where authors show the superiority of the EARSM model in capturing secondary flows in the case of backward facing step. The reason can be in the origins of secondary flows which are driven by the anisotropy of Reynolds stress tensor in the case of backward facing steps whereas the interaction of inlet boundary layer with the inlet edge together with pressure gradient coming from the centrifugal force are much more important for the flows through turbine cascade.

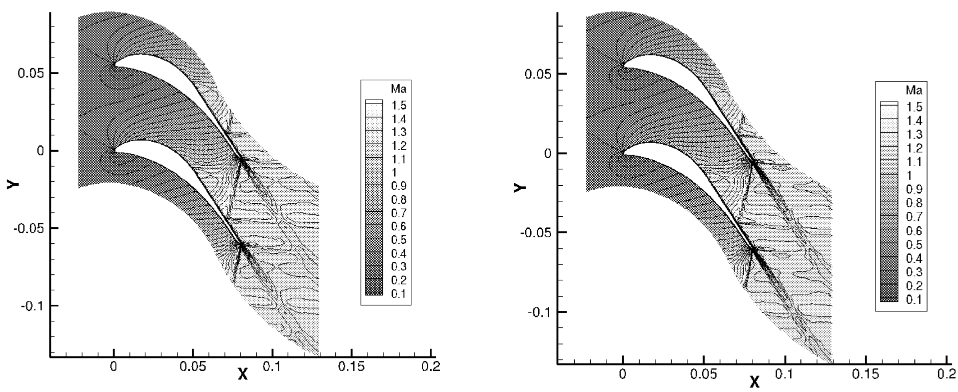

(a) Symmetry plane, 3D, unstructured mesh

(b) Symmetry plane, 3D, locally refined mesh

Fig.2: The Mach number in the symmetry plane computed with SST model using unstructured and locally refined mesh

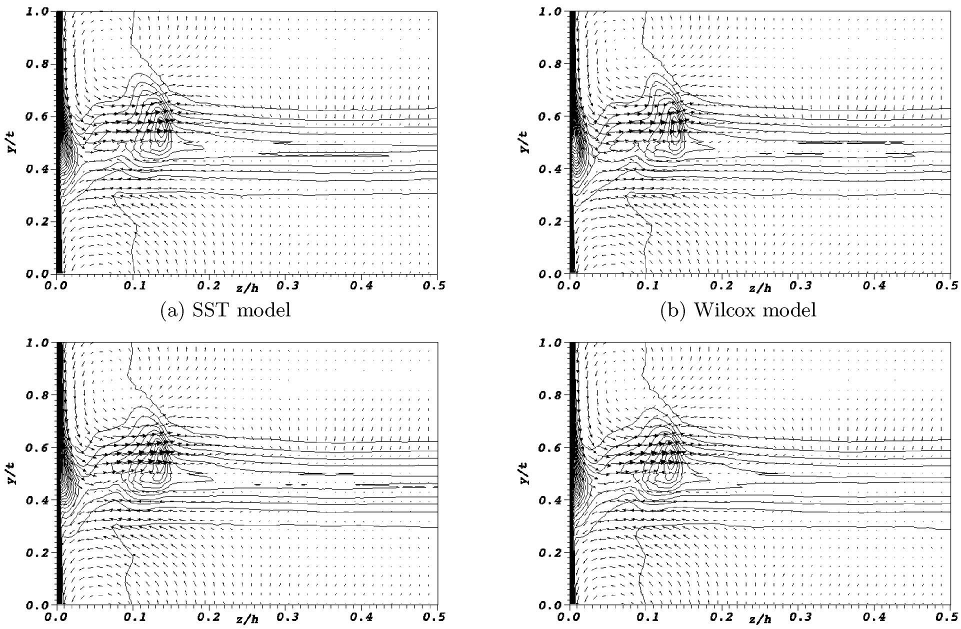

(a) SST model (b) Wilcox model

(c) TNT model with vortex modification (d) EARSM model

Fig.3: The isolines of local kinetic energy loss coeeficient and the structure of secondary flows in the traversing plane

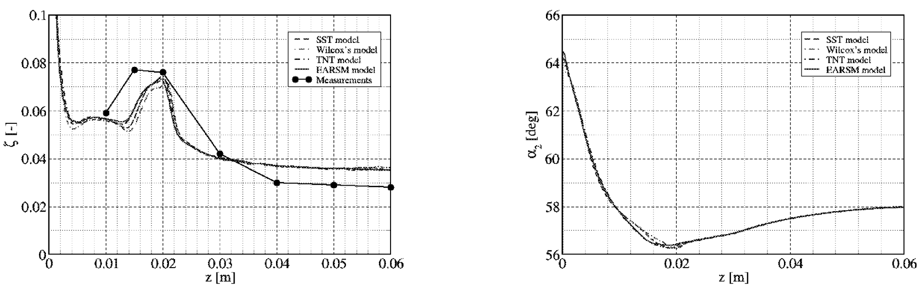

(a) Loss coefficient ζ (b) Outlet angle α_2

Fig.4: Spanwise distribution of the kinetic energy loss coefficient and the outlet angle

The figure 4 shows the spanwise distribution of ζ and outlet angle α_2 obtained with all four models. There are small differences between all models. The Wilcox's model predicts slightly lower losses than other models. On the other hand the simple TNT model of Brandsma et al. [1] and the EARSM model of Wallin [14] give almost identical results. Note that all models used in this study are based on the solution of two equations for turbulent kinetic energy k and specific dissipation rate ω. With the exception of SST model the equations stem from the original Wilcox's $k-\omega$ model whereas the SST model uses as its base a combination of $k-\omega$ and $k-\varepsilon$ models.

4. Conclusion

The span-wise distribution of the energy losses was studied for the case of prismatic turbine cascade in the transonic regime. Numerical simulations with different turbulence models show that the effect of the choice of turbulence model has much less important influence on the energy losses and the secondary flows than the specification boundary layer thickness in the inlet channel studied in Fürst, Luxa, and Šimurda [3].

The comparison of numerical simulation with experimental data shows that the CFD simulation is capable of qualitatively resolve basic 3D flow effects. In accordance with findings made by Lampart [7], the numerical simulations overpredict the level of energy losses in the wake in the middle part of the channel. This can be caused by the fact that the current turbulence models don't account for laminar-turbulent transition whereas the real flow is probably laminar at certain part of the blade, see e.g. Straka and Příhoda [13]. On the other hand the level of losses in near-wall flow is under-predicted with respect to the experiment which is in contrary with results of Lampart [7] obtained for subsonic flows.

Acknowledgment

The work was supported by the Grant no. P101/10/1329 of the Czech Science Foundation.

References

[1] Brandsma F. et al.: Leading edge vortex ow computations and comparison with DNW-HST wind tunnel data, Tech. rep. NLR-TP-2001-238, National Aerospace Laboratory NLR, 2001
[2] Ferziger J.H., Peric M.: Computational Methods for Fluid Dynamics, Springer, 1999
[3] Fürst J., Luxa M., Šimurda D: Span-wise Distribution of Losses in Prismatic Turbine Cascade, In: 19th International Conference Engineering Mechanics 2013. Institute of Thermomechanics, AS CR v.v.i., 2013
[4] Kok J.C.: Resolving the dependence on free stream values for the k-ω turbulence model, In: AIAA Journal 38 (2000), pp. 1292–1295
[5] Kozel K., Příhoda J.: ERCOFTAC QNET-CFD, 2004 http://qnet-ercoftac.cfms.org.uk/w/index.php/Silver:AC_6-12_Description
[6] Kozel K., Louda P., Příhoda J.: Numerical solution of 2D and 3D backward facing step ows, In: PAMM 5.1 (2005), pp. 467–468
[7] Lampart P.: Investigation of Endwall Flows and Losses in Axial Turbines. Part I. Formation of Endwall Flows and Losses, In: J. of Theoretical and Applied Mechanics 47.2 (2009), pp. 321–342
[8] Lampart P.: Investigation of Endwall Flows and Losses in Axial Turbines. Part II. The Effect of Geometrical and Flow Parameters, In: J. of Theoretical and Applied Mechanics 47.4 (2009), pp. 829–853 Luxa M. et al.: Causes and solution of aperiodicity of supersonic ow field downstream of a profile cascade, In: Communications 14/4a (2012), pp. 23–28, ISSN 1335-4205
[9] Matějka M. et al.: Loss Coeficient Dependence of Turbine Blade Cascade, In: ASME Paper GT2010-22740 (2010)
[10] Menter F.R.: Two-Equation Eddy-Viscosity Turbulence Models for Engeenering Applications, In: AIAA J. 8.32 (1994), pp. 1598–1605
[11] Sieverding C.H.: Recent Progress in the Understanding of Basic Aspects of Secondary Flows in Turbine Blade Passages, In: ASME J. Turbomach. 107 (1985), pp. 249–257
[12] Straka P., Příhoda J.: Application of the algebraic bypass-transition model for internal and external ows, In: Proc Conf. Experimental Fluid Mechanics (EFM10), TU Liberec, 2010, pp. 636–641
[13] Wallin S.: Engineering turbulence modelling for CFD with a focus on explicit algebraic Reynolds stress models, PhD thesis, Stockholm: Royal Institute of Technology, 2000

[14] Wilcox D.C.: Formulation of the $k - \omega$ Turbulence Model Revisited, In: AIAA 46.11 (2008), pp. 2823–2838
[15] Šafařík P. et al.: Data Reduction Method for Three-Dimensional Transonic Flow Measurements, In: Symposium on measuring techniques in transonic and supersonic ow in cascades and turbomachines, Royal Institute of Technology. Stockholm, 2004, pp. 8–9
[16] Šťastný M., Šafařík P.: Experimental Analysis Data on the Transsonic Flow Past a Plane Turbine Cascade, In: ASME Paper 90-GT-313 (1990)

Received in editor's office: July 26, 2013
Approved for publishing: November 4, 2013